Isovector spin susceptibility: Isotopic evolution of collectivity in spin response

Kenichi Yoshida ●*

Department of Physics, Kyoto University, Kyoto 606-8502, Japan

Background: Response to spin-dependent operators has been investigated in the magnetic dipole and Gamow-Teller transitions that provide magnetic properties of a nuclear system.

Purpose: I investigate an isotopic dependence of the collectivity generated by the spin-dependent interactions in the Ca and Ni isotopes through the isovector- (IV-) spin-flip excitations. The responses in the neutral (t_z) and charge-exchange ($t_\pm$) channels are considered in a unified way.

Method: A nuclear energy-density functional approach is employed for calculating the response functions based on the Skyrme-Kohn-Sham-Bogoliubov method and the quasiparticle-random-phase approximation (QRPA). I adopt the like-particle QRPA and the proton-neutron QRPA for the neutral and charge-exchange channels, respectively. I consider the fluctuation of the proton-neutron pair fields.

Results: The collective shift due to RPA correlations for the response in the neutral channel is explained by the occupation probability of neutrons in the $j_> = \ell + 1/2$ orbital. Many particle-hole or two-quasiparticle excitations have a coherent contribution to form a giant resonance in neutron-rich nuclei for the charge-exchange channel. The IV-spin susceptibility displays the isotopic evolution of the collectivity and the underlying shell structure.

Conclusions: A repulsive character of the residual interaction in the spin-isospin channel diminishes the IV-spin susceptibility due to the collectivity, whereas the dynamic ^3S pairing appearing in the charge-exchange channel opposes the reduction.

I. INTRODUCTION

Susceptibility to an applied magnetic field is a fundamental property characterizing the matter. A detailed investigation unveils the single-particle and collective behavior of the spin degree of freedom. An interplay of superconductivity and magnetism has attracted much interest and has been a central issue in strongly correlated many-body systems [1]. The fermionic superfluidity or superconductivity is well understood by the $^1S_0$ pair correlation mostly [2,3]. The onset of the spin susceptibility below the critical temperature is a manifestation of the spin-triplet ($S = 1$) superfluidity of ^{3}He [4,5]. The $S = 1$ pairing in electronic systems has been investigated not only in the superfluid ^{3}He [6], but also in other systems recently [7,8]. In contrast, there has been a continuing discussion on the $S = 1$ pairing in nuclear systems: the $^3S_1$ correlation of isoscalar (IS) proton-neutron (pn) pairs in $N \sim Z$ nuclei [9] and the $^3P_2$ pairing of neutrons in the neutron-star matter [10].

Response of a nucleus to an external field displays the correlations among constituent nucleons. The nuclear response is characterized by the transferred angular momentum ΔL, spin ΔS, isospin ΔT, and nucleon number ΔN [11]. The response categorized as $\Delta L = 0$, $\Delta S = 0$, $\Delta T = 1$, $\Delta N = 2$ pins down the $^1S_0$ pairing [3], and the response

$\Delta L = 0$, $\Delta S = 1$, $\Delta T = 0$, $\Delta N = 2$ has been studied recently to uncover the $^3S_1$ pairing [12–14]. The response to the spin-dependent electromagnetic and weak probes reveals the magnetic properties of nuclear matter [15–17]. The isovector- (IV-) spin magnetic-dipole (M1) response with $\Delta L = 0$, $\Delta S = 1$, $\Delta T = 1$, $\Delta N = 0$ has been investigated extensively because they impact diverse quantities, such as the neutral-current neutrino-nucleus cross sections relevant to supernova physics and neutrino physics [18] and the neutron-capture cross sections relevant to the nucleosynthesis [19–21]. Furthermore, the IV-spin-M1 response can be seen in a wider perspective when it is considered as a single component $\Delta T_z = 0$ of the IV modes [22]. The additional components $\Delta T_z = \pm 1$ represent the charge-exchange modes, namely, the Gamow-Teller (GT) response.

The GT response can be a probe to disclose the $^3S_1$ IS pairing. The dynamic IS pairing lowers the GT states in energy and, thus, shortens the β-decay half-lives of neutron-rich nuclei [23] including deformed nuclei [24]. The effects of the IS pairing on the GT transition strengths have been studied in $N = Z$ odd-odd nuclei with a three-body model of two nucleons around a spherical core [25]. A remarkable feature found in $N = Z$ odd-odd nuclei with an LS-closed core (^{4}He, ^{16}O, ^{40}Ca) is the appearance of the low-energy state with a strong GT strength. A similar trait is also found by employing a microscopic nuclear energy-density functional (EDF) method [26]. The low-energy GT states have been

———————
*kyoshida@ruby.scphys.kyoto-u.ac.jp

indeed identified experimentally in the transitions of $^{18}\text{O} \rightarrow$ ^{18}F [27] and $^{42}\text{Ca} \rightarrow$ ^{42}Sc [28,29].

In this article, I am going to investigate the collectivity generated by the spin response in view of the pair correlations. An isotopic dependence is studied to see the shell effects. To this end, the EDF method is employed: A theoretical model capable of handling nuclides with an arbitrary mass number in a single framework [30,31]. I introduce and evaluate the IV-spin susceptibility to discuss the neutron number dependence of the magnetic property quantitatively.

This paper is organized in the following way: The theoretical framework for describing the spin responses is given in Sec. II and details of the numerical calculation are also given; Sec. III is devoted to the numerical results and discussion based on the model calculation; the discussion on the response of the Ca isotopes in the neutral and charge-exchange channels is given in Secs. III A and III B, respectively; the discussion for the Ni isotopes is given in Sec. III C; then, a summary is given in Sec. IV.

II. FRAMEWORK

A. Kohn-Sham-Bogoliubov and quasiparticle-random-phase approximation for neutron-rich nuclei

Since the details of the formalism can be found in Refs. [24,32,33], here I briefly recapitulate the basic equations relevant to the present paper. In the framework of the nuclear EDF method I employ, the ground state of a mother (target) nucleus is described by solving the Kohn-Sham-Bogoliubov (KSB) equation [34],

$$\sum_{s'} \begin{bmatrix} h_{ss'}^q(\boldsymbol{r}) - \lambda^q \delta_{ss'} & \tilde{h}_{ss'}^q(\boldsymbol{r}) \\ \tilde{h}_{ss'}^q(\boldsymbol{r}) & -h_{ss'}^q(\boldsymbol{r}) + \lambda^q \delta_{ss'} \end{bmatrix} \begin{bmatrix} \varphi_{1,\alpha}^q(\boldsymbol{r}s') \\ \varphi_{2,\alpha}^q(\boldsymbol{r}s') \end{bmatrix}$$
$$= E_\alpha \begin{bmatrix} \varphi_{1,\alpha}^q(\boldsymbol{r}s) \\ \varphi_{2,\alpha}^q(\boldsymbol{r}s) \end{bmatrix}, \tag{1}$$

where the single-particle and pair Hamiltonians $h_{ss'}^q(\boldsymbol{r})$ and $\tilde{h}_{ss'}^q(\boldsymbol{r})$ are given by the functional derivative of the EDF with respect to the particle density and the pair density, respectively. An explicit expression of the Hamiltonians is found in the Appendix of Ref. [35]. The superscript q denotes ν (neutron, $t_z = 1/2$) or π (proton, $t_z = -1/2$). The average particle number is fixed at the desired value by adjusting the chemical potential λ^q. When neutrons and/or protons are unpaired, the chemical potential is adapted to lie in the center of the highest occupied and the lowest unoccupied orbitals. Assuming the system is axially symmetric, the KSB equation (1) is block diagonalized according to the quantum number Ω, the z component of the angular momentum.

The excited states $|i\rangle$ are described as one-phonon excitations built on the ground-state $|0\rangle$ of the mother nucleus as

$$|i\rangle = \hat{\Gamma}_i^\dagger |0\rangle, \tag{2}$$

$$\hat{\Gamma}_i^\dagger = \sum_{\alpha\beta} \{ X_{\alpha\beta}^i \hat{a}_\alpha^\dagger \hat{a}_\beta^\dagger - Y_{\alpha\beta}^i \hat{a}_{\bar{\beta}} \hat{a}_{\bar{\alpha}} \}, \tag{3}$$

where $\hat{a}^\dagger$ and $\hat{a}$ are the quasiparticle (qp) creation and annihilation operators that are defined in terms of the solutions

of the KSB equation (1) with the Bogoliubov transformation. The phonon states, the amplitudes X^i, Y^i and the vibrational frequency ω_i, are obtained in the quasiparticle-random-phase approximation (QRPA): the linearized time-dependent density-functional theory for superfluid systems [31]. The EDF gives the residual interactions entering into the QRPA equation. For the axially symmetric nuclei, the QRPA equation is block diagonalized according to the quantum number $K = \Omega_\alpha + \Omega_\beta$. The deformed QRPA developed in Refs. [32,33] is extended to describe the response to the spin-dependent operators.

B. Numerical procedures

To describe the developed neutron skin and the neutrons pair correlation coupled with the continuum states that emerge uniquely in neutron-rich nuclei, I solve the KSB equation in the coordinate space using cylindrical coordinates $\boldsymbol{r} = (\rho, z, \phi)$ with a mesh size of $\Delta\rho = \Delta z = 0.6$ fm and a box boundary condition at $(\rho_{\max}, z_{\max}) = (14.7, 14.4)$ fm. Since I assume further the reflection symmetry, only the region of $z \geqslant 0$ is considered. The qp states are truncated according to the qp energy cutoff at 70 MeV, and the qp states up to the magnetic quantum number $\Omega = 23/2$ with positive and negative parities are included. I introduce the truncation for the two-quasiparticle (2qp) configurations in the QRPA calculations, in terms of the 2qp energy as 60 MeV.

For the normal [particle–hole, (p–h)] part of the EDF, I mainly employ the SGII functional [36]. To complement the discussion, I use the SkP functional [34] which has a different spin-isospin property to SGII. For the pairing energy, I adopt the one in Ref. [37] that depends on both the IS and the IV densities in addition to the pair density with the parameters given in Table III of Ref. [37]. The same pairing EDF is employed for the ^1S pn pairing in the proton-neutron QRPA (pnQRPA) calculation, whereas the linear term in the IV density is dropped. The effect of the dynamic IS ($T = 0$) paring is investigated by changing the strength of the interaction. Note that the pnQRPA calculations including the dynamic IS pairing with more or less the same strength as the ^1S pairing describe well the characteristic low-lying GT strength distributions in the light $N \simeq Z$ nuclei [27–29].

III. RESULTS AND DISCUSSION

I consider the response of the Ca isotopes with the mass number $A = 42$–70 and the Ni isotopes with $A = 52$–78 to the IV-spin-flip operator defined by

$$\vec{F}_K = \mu \frac{1}{\sqrt{2}} \sum_{ss'} \sum_{tt'} \int d\boldsymbol{r} \, \psi^\dagger(\boldsymbol{r}s't') \psi(\boldsymbol{r}st) \langle s'|\sigma_K|s\rangle \langle t'|\vec{\tau}|t\rangle, \tag{4}$$

where $\mu = \mu_\text{N}(g_\nu - g_\pi)$ with $\mu_\text{N} = e\hbar/2mc$ being the nuclear magneton g_ν, g_π the spin g factor of a neutron and a proton and σ_K and $\vec{\tau} = (\tau_{+1}, \tau_0, \tau_{-1})$ denote the spherical components of the Pauli matrix of spin and isospin. With this operator, the spin modes of the neutral (isospin unchanging: τ_0) and isospin changing ($\tau_{\pm 1}$) excitations are investigated in a unified way. Note that I use here a probing operator that is
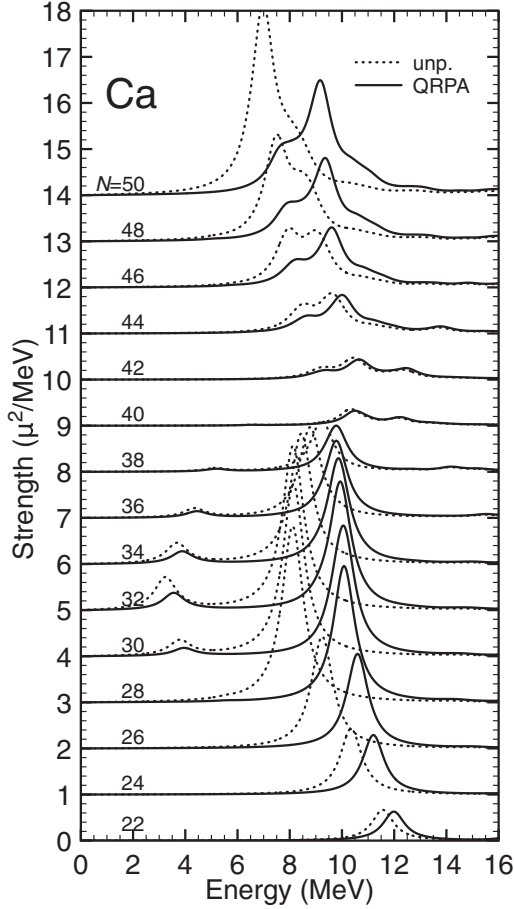
FIG. 1. Calculated distributions (shifted) of the IV-spin-flip transition strengths in the neutral channel as functions of the excitation energy by employing the SGII functional. The smearing parameter $\gamma = 1$ MeV is used. The results obtained without the RPA correlations (unp.) are depicted by the dotted lines.

$\mu\sqrt{2\pi}$ times the one used in Ref. [22]. The IV-spin-M1 and GT operators are indeed related to the IV-spin-flip operator (4) as $F_K^{\mathrm{IV,s}}(\mathrm{M1}) = \sqrt{\frac{3}{8\pi}}F_{K,0}$ and $\vec{F}_K(\mathrm{GT}) = \frac{g_A}{\mu}\vec{F}_K$ when the contribution of the meson-exchange and isobar currents is discarded [38,39]. Here g_A is the axial-vector coupling constant.

The Ca and Ni isotopes are all spherical in the ground state within the present model. The neutrons are paired in all the isotopes except ^{70}Ca, ^{56}Ni, and ^{78}Ni whereas the protons are unpaired except in ^{52}Ni.

A. Neutral channel: IV-spin-M1 states in Ca isotopes

According to the shell model, in a spin-saturated closed-shell nucleus, such as ^{40}Ca, the M1 excitations are forbidden to occur. Thus, the spin-flip excitations in the Ca isotopes that I investigate here are by virtue of the excitation of neutrons. It is noted, however, that the M1 strengths in ^{40}Ca were observed around 10 MeV [40] and the beyond-RPA correlation is indispensable to describe such a forbidden state [41].
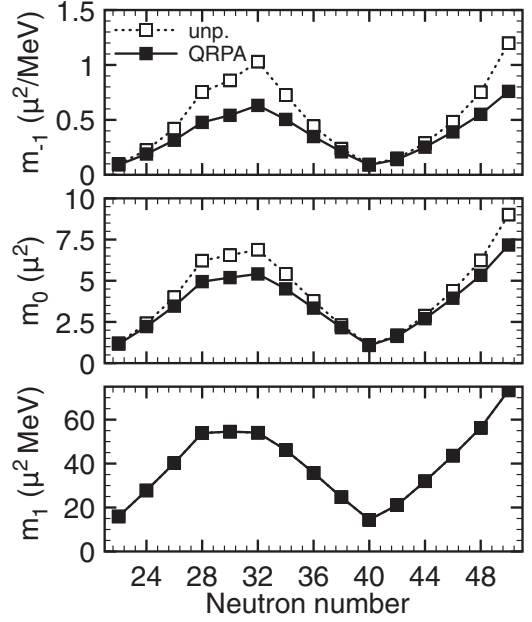

FIG. 2. Moments m_k ($k = -1$, 0, and 1) of the transition strengths in the Ca isotopes as functions of the neutron number. The results obtained without the RPA correlations (unp.) are depicted by the dotted lines with open symbols.

Figure 1 shows the calculated transition strengths for the IV-spin-flip excitation in the neutral channel, corresponding to the IV-spin-M1 excitation:

$$S(E) = \sum_{K=-1}^{1} \frac{dB(E, F_K)}{dE}, \qquad (5)$$

$$\frac{dB(E, F_K)}{dE} = \frac{2E\gamma}{\pi} \sum_i \frac{\tilde{E}_i |\langle i|F_{K,0}|0\rangle|^2}{\left(E^2 - \tilde{E}_i^2\right)^2 + E^2\gamma^2}, \qquad (6)$$

where $\tilde{E}_i^2 = (\hbar\omega_i)^2 + \gamma^2/4$ [42]. The smearing width γ is set to 1 MeV, which is supposed to simulate the spreading effect $\Gamma^\downarrow$ missing in the QRPA.

In the $^{42-48}$Ca isotopes, the spin-M1 resonant state is generated by the $\nu f_{7/2} \to \nu f_{5/2}$ excitation. The unperturbed state is shifted up in energy due to the residual interaction of the $\sigma_1\sigma_2\tau_1\tau_2$ type. To discuss the isotopic dependence of the strength distributions quantitatively, I show in Fig. 2 the moment of the strengths defined by

$$m_k = \sum_K \sum_i (\hbar\omega_i)^k |\langle i|F_{K,0}|0\rangle|^2 \qquad (7)$$

for $k = -1$, 0, and 1. A linear rise seen in m_0 from ^{42}Ca to ^{48}Ca is understood by the occupation of neutrons in the $f_{7/2}$ orbital. A p-h-type transition strength is proportional to u^2v^2 of the Bardeen-Cooper-Schrieffer (BCS) amplitude. Since the $f_{5/2}$ orbital is completely empty $u_{f_{5/2}} = 1$, the transition strengths develop monotonically as $v_{f_{7/2}}^2$ increases. Here, the occupation probability v_α^2 can be evaluated by $\int d\mathbf{r} \sum_s |\varphi_{2,\alpha}(\mathbf{r}s)|^2$ using the qp wave functions. Comparing the results with and those without the RPA correlations, the effect of RPA correlations is also enhanced from ^{42}Ca to

^{48}Ca. The mean excitation energy evaluated by m_1/m_0 with (without) the RPA correlations is 13.8 (13.2), 12.5 (11.5), 11.6 (10.1), and 10.9 (8.7) MeV for ^{42,44,46,48}Ca, respectively. This is again due to a gradual occupation of neutrons in the $f_{7/2}$ orbital. A two-body matrix element entering the QRPA equation is approximately proportional to $uvuv$ of the BCS amplitude. In the present case, only the $\nu f_{7/2} \to \nu f_{5/2}$ excitation accounts for the appearance of spin-M1 resonance in essence. Thus, the energy shift is due to the diagonal matrix element, which is proportional to $u^2_{f_{5/2}} v^2_{f_{7/2}}$ and evidently the occupation number of neutrons in the $f_{7/2}$ orbital.

Experimentally, the 1^+ state at 11.2 and 10.3 MeV in ^{42}Ca and ^{48}Ca was populated by the inelastic electron scattering [43]. In the present model, the IV-spin M1 strength is concentrated on the 1^+ state at 11.2 and 10.1 MeV in ^{42}Ca and ^{48}Ca. A good agreement with the experiment shows the validity of the theoretical calculations.

One sees an onset of the low-energy state in $^{50-56}$Ca. This is due to the $\nu p_{3/2} \to \nu p_{1/2}$ excitation. The increase in m_0 from ^{50}Ca to ^{52}Ca is understood by the occupation of neutrons in the $p_{3/2}$ orbital similarly in the case of the $f_{7/2}$ orbital in $^{42-48}$Ca. When the neutron number increases further, neutrons start to occupy the $p_{1/2}$ orbital. Then, the occupation of neutrons in the $p_{1/2}$ orbital diminishes the transition strength as $u^2_{p_{1/2}} v^2_{p_{3/2}} = 1 - v^2_{p_{1/2}}$. A linear reduction in m_0 and the energy shift due to the RPA correlations is seen up to ^{60}Ca where the occupation of neutrons in the $f_{5/2}$ orbital is fulfilled. Note that the $f_{5/2}$ orbital is bound although the separation energy $E_{f_{5/2}} - \lambda^\nu$ is low as 1.4 MeV. In ^{60}Ca, the spin excitation is forbidden. A tiny strength, however, appears in the calculation. The appearance of the strengths is due to the pairing of neutrons. In the present calculation, the occupation probability of the $\nu 1g_{9/2}$ orbital is 0.08.

Beyond ^{60}Ca, a linear increase in m_0 and the energy shift due to the RPA correlations is mainly due to a gradual occupation of neutrons in the $1g_{9/2}$ orbital. A distinct feature in the neuron-rich nuclei beyond $N = 40$ is that the $g_{7/2}$ orbital is no more a bound state. Furthermore, there can be an appreciable contribution of 2qp excitations in the continuum because the resonance shape is not simply a single peak as calculated below $N = 40$. Therefore, the spin-M1 state acquires a wider width due to a stronger coupling to the continuum states. Since the continuum states are discretized in the present calculation, a quantitative discussion on the resonance shape is not easy. It is, thus, an interacting future work to extend the continuum calculation, such as in Ref. [44] to heavier nuclei and discuss the neutron-number dependence of the width of the spin-M1 resonance [45]. The evolution of the spin-M1 strength distributions in the Ca isotopes is similar to the one predicted by the relativistic EDF approach [46]. It is noted that the pairing governing the isotopic dependence of the RPA correlations in the spin-M1 excitation is the static pairing effect. The dynamic pairing caused by the residual pair interaction does not affect the collectivity of the unnatural parity states in the present model, whereas it enhances the collectivity of the natural parity states as discussed, e.g., in Refs. [47–52].

The inverse energy-weighted sum m_{-1} shown in Fig. 2 is related to the IV-spin susceptibility

[53] as

$$\chi_z \equiv 2\mu^2 \sum_i \frac{|\langle i|S_z T_z|0\rangle|^2}{\hbar\omega_i} = \frac{m_{-1}}{3}, \tag{8}$$

where $S_z T_z = \int d\boldsymbol{r} \sum \psi^\dagger(\boldsymbol{r}s't') \psi(\boldsymbol{r}st) \langle s'|\frac{\sigma_z}{2}|s\rangle \langle t'|\tau_0|t\rangle$. This is of particular interest because it is not sensitive to the high-energy side of the response and, hence, is less affected by the two-particle–two-hole (2p2h) excitations [15]. For nuclear matter, the IV magnetic susceptibility per nucleon is simply expressed [54] as

$$\bar{\chi}_z = \frac{1 + \frac{1}{3}F_1}{1 + G_0'} \mu^2 N_0, \tag{9}$$

with the Landau parameters N_0, G_0', and F_1 and $\mu^2 N_0$ is regarded as the Pauli paramagnetic susceptibility. The susceptibility of the correlated systems is suppressed due to the repulsive nature of the interaction $G_0' > 0$. Note that the unperturbed value displayed in the top panel of Fig. 2 includes the effect of F_1, i.e., the effective mass that reduces the susceptibility and the like-particle pairing that also reduces the susceptibility as for the Belyaev inertia [55]. In the present case for the Ca isotopes since protons do not take part in generating the collectivity, the spin-M1 state is simply described as a neutron p-h excitation of the spin-orbit partners. Therefore, the reduction of the susceptibility strongly depends on the shell structure and the pairing correlation of neutrons. The effect of the residual interaction is seen more clearly than in m_{-1}.

B. Charge-exchange channel: GT states in Ca isotopes

Figure 3 shows the calculated transition strengths for the IV-spin-flip excitation in the charge-exchange channel (t_-), corresponding to the GT excitation as given similarly to Eqs. (5) and (6) except by replacing the excitation energy E with $E_T = E - \lambda^\nu + \lambda^\pi$ so that the excitation is with respect to the ground state of the mother (target) nucleus. The transition in the t_+ channel is strongly suppressed as the excitation of protons in the neutral channel.

Let me discuss the GT excitations in $^{42-48}$Ca shown in Fig. 3(a). One sees a two-hump structure whereas there is only a single peak in the spin-M1 response. These states are mainly constructed by the $\nu f_{7/2} \to \pi f_{7/2}$ and $\nu f_{7/2} \to \pi f_{5/2}$ configurations. Since the $(\nu f_{7/2})^2$ configuration couples to $S = 0$, this does not take part in the formation of the spin-M1 state. With the growth of the neutron number, the transition strength increases. This is understood by a gradual increase in the occupation of neutrons in the $f_{7/2}$ orbital as discussed for a linear rise in the transition strengths in the neutral channel. The excitation energy is predominantly given by the unperturbed energy and the diagonal matrix element of the $\sigma_1\sigma_2\tau_1\tau_2$ interaction, and the two peaks are shifted up in energy due to a repulsive character of the interaction. The energy shift is also nearly proportional to the occupied neutron number in the $f_{7/2}$ orbital.

The IS pairing affects the GT states [23,24] and explains well the enhancement of the strength for the low-energy GT state in ^{18}O (^{42}Ca) [26–29,56] where the particle-particle (p-p) type excitations of $\nu p_{3/2} \to \pi p_{3/2}$ ($\nu f_{7/2} \to \pi f_{7/2}$) and
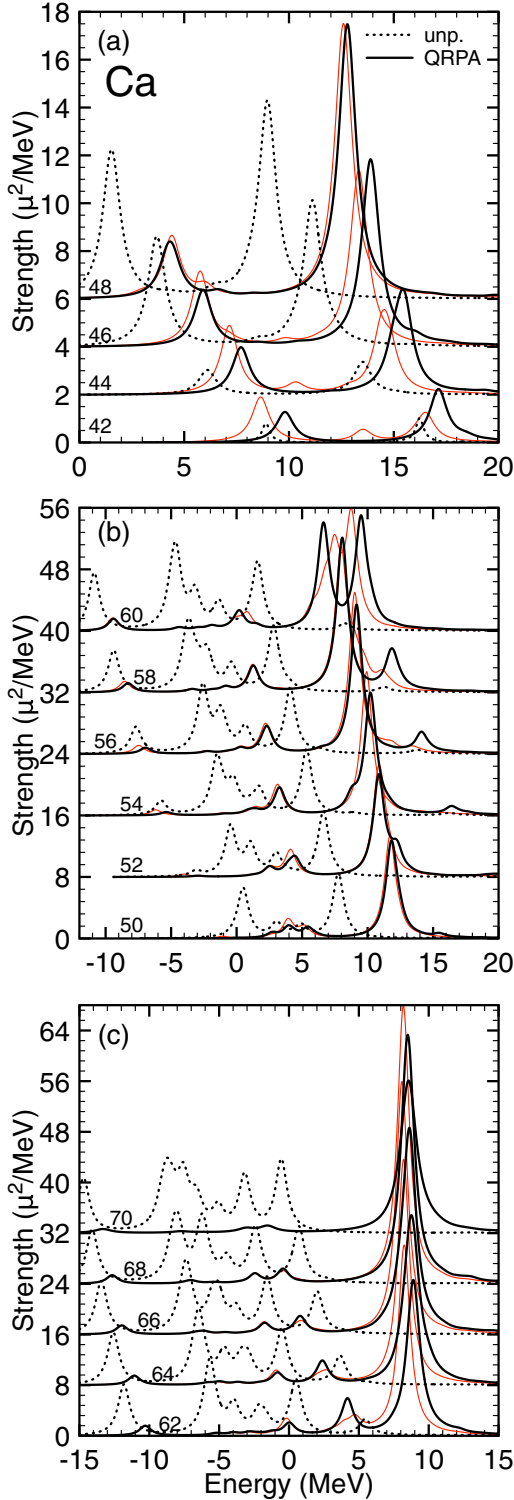
FIG. 3. Similar to Fig. 1 but for the response to the t^- channel of the operator (4) in (a) $^{42-48}$Ca ($f_{7/2}$ shell), (b) $^{50-60}$Ca ($p - f_{5/2}$ shell) and (c) $^{62-70}$Ca ($g_{9/2}$ shell). The results including the $T = 0$ (spin-triplet) pairing are drawn by the thin lines.

$\nu p_{3/2} \to \pi p_{1/2}$ ($\nu f_{7/2} \to \pi f_{5/2}$) cooperatively participate in generating the low-energy GT state. The numerical results including the dynamic IS pairing are depicted by the thin line in Fig. 3. The effect of the IS pairing is strong in ^{42}Ca as

discussed in Ref. [26]. Here, the strength of the IS pair interaction was set as the same as that for the IV pair interaction.

Experimentally, the GT strength is concentrated on the 1^+ state at 0.61 MeV in ^{42}Sc, that is observed by the ^{42}Ca(^{3}He, t) reaction [28,29]. In the present model, the 1^+ state appears at 1.79 MeV above the isobaric analog state (IAS) (the ground state of ^{42}Sc). With the IS pair interaction being included, I obtain the 1^+ state at 0.63 MeV. In the ^{44}Ca(^{3}He, t) ^{44}Sc reaction, the 1^+ state was observed at 2.11 MeV below the IAS [57]. The calculation gives the 1^+ state at 0.38 MeV above and 0.17 MeV below the IAS without and with the IS pair interaction, respectively. The IS pairing is still active, but the effect is weaker than in ^{42}Ca. In the ^{48}Ca(^{3}He, t) ^{48}Sc reaction, the 1^+ state was observed at 4.18 MeV below the IAS [58]. The calculation gives several 1^+ states in low energies: 2.4–2.6 MeV below the IAS.

As neutrons occupy the $2p$ orbitals, the $\nu p_{3/2,1/2} \to \pi p_{3/2,1/2}$ excitations show up in low energies as depicted by the dotted lines in Fig. 3(b). Thanks to the RPA correlations, most of the strengths are gathered into the giant resonance though there remains a tiny strength in the low-energy region. These low-lying states are responsible for the β decay.

Beyond $N = 34$, one sees an appreciable amount of the unperturbed strengths is developed in low energies with an increase in the neutron number. This comes from the $\nu f_{5/2} \to \pi f_{7/2}$ excitation. Due to the RPA correlations, however, most of the strengths are brought together into the high-lying giant resonance. The remaining low-lying state is expected to be affected by the IS pairing because of the p-p nature of the configuration. In ^{54,56}Ca, the occupation probability of neutrons in the $f_{5/2}$ orbital is 0.2 and 0.4. In the present cases, the low-lying state is lowered in energy and enhanced in strengths only slightly as shown by the thick line in Fig. 3(b). This is because the $\nu f_{7/2} \to \pi f_{5/2}$ excitation is purely a p-h type and is not affected by the IS pairing.

The IS pairing affects the giant resonance as neutrons partially occupy the $g_{9/2}$ orbital. Beyond $N = 40$, the $\nu g_{9/2} \to \pi g_{9/2}$ configuration appears more clearly in the high-energy region according to a gradual increase in the occupation probability of neutrons in the $g_{9/2}$ orbital. Since this configuration is a p-p type excitation, the IS pairing is active. As one can see in Fig. 3(c), the giant resonance is lowered in energy due to the attractive nature of the IS pairing.

In neutron-rich isotopes, the number of the available p-h or 2qp excitations increases because of the imbalanced Fermi level of neutrons and protons. Therefore, the GT strengths are concentrated in the giant resonance in $^{62-70}$Ca as a collective effect notwithstanding that a significant fraction of the GT strengths is found inside the Q_β window without the RPA correlations. The superallowed GT resonance predicted in the light neutron drip-line nuclei [59] is, thus, unlikely to occur in the Ca isotopes even near the drip line.

To investigate the magnetic property systematically, I introduce the static susceptibility. The IV-spin susceptibility in the charge-exchange channel is given as

$$\chi_\perp = \mu^2 \left[\sum_i \frac{|\langle i|S_z T_-|0\rangle|^2}{\hbar\omega_i} + \sum_i \frac{|\langle i|S_z T_+|0\rangle|^2}{\hbar\omega_i} \right], \quad (10)$$
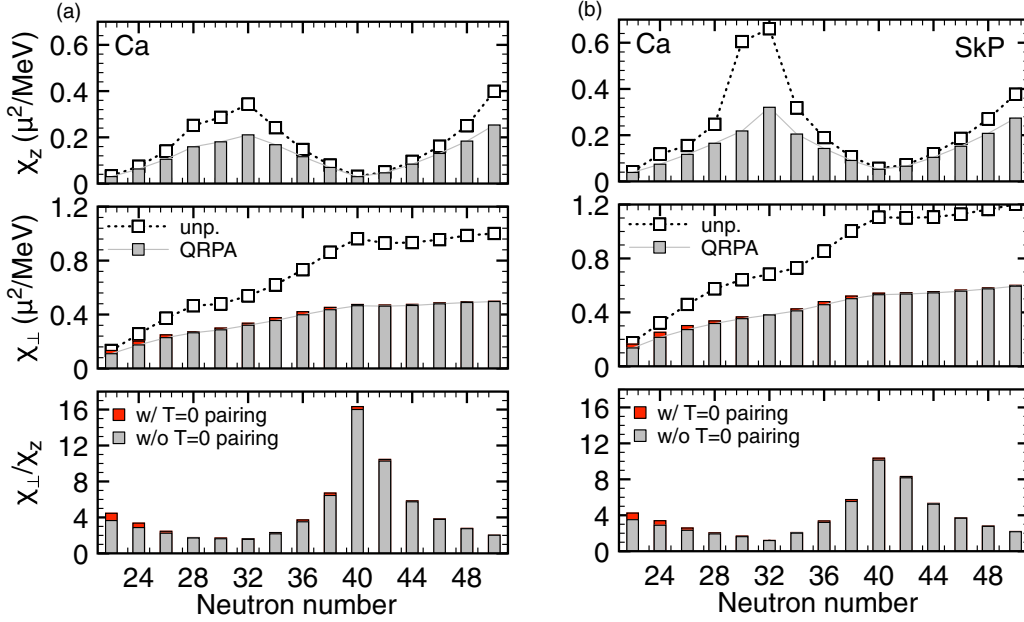
FIG. 4. Results obtained by using the (a) SGII functional and (b) SkP functional. Top: IV-spin susceptibility χ_z of the Ca isotopes obtained with and without the RPA correlations. Middle: IV-spin susceptibility $\chi_\perp$ in the charge-exchange channel. Bottom: Ratio of the IV-spin susceptibilities $\chi_\perp/\chi_z$ obtained with and without the dynamic $T = 0$ (spin-triplet) pairing.

where $S_z T_\pm = \int d\mathbf{r} \sum \psi^\dagger(\mathbf{r}s't')\psi(\mathbf{r}st)\langle s'|\frac{\sigma_z}{2}|s\rangle\langle t'|\tau_{\pm 1}|t\rangle$. For nuclear matter, one may expect $\chi_\perp$ coincides with χ_z. The IV-spin susceptibility in the charge-exchange channel is reduced due to the RPA correlations as in the neutral channel.

I show in the middle panel of Fig. 4(a) the calculated IV-spin susceptibilities $\chi_\perp$ obtained with and without the RPA correlations. As the neutron number increases, the p-h or 2qp excitations possessing the nonvanishing GT matrix-element appear in low energies. The susceptibility in the free system, thus, increases. Since the operator (4) changes only the direction of spin and isospin and does not change the spatial structure, the p-h or 2qp configurations in the $0\hbar\omega_0$ excitation are only possible to appear in the GT response. Around $N = 40$, the $-1\hbar\omega_0$ excitations start to appear in low energies [60], and the $0\hbar\omega_0$ excitations show up in a relatively higher-energy region. Therefore, $\chi_\perp$ keeps almost unchanged beyond $N = 40$. The effect of the RPA correlations becomes apparent as the collectivity becomes strong. With an increase in the neutron number, the number of p-h or 2qp excitations in the pf shell increases, and they make a coherent contribution to the formation of the giant resonance. One can, thus, see a systematic reduction of $\chi_\perp$ from the unperturbed one in the range of $22 \leqslant N \leqslant 40$.

The dynamic IS pairing acts on the spin response oppositely to the p-h residual interaction, the former causes an attractive shift of the transitions and enhances the susceptibility whereas the latter a repulsive shift and reduces the susceptibility. For nuclear matter one may assume to express the ratio of the IV-spin susceptibilities as

$$\frac{\chi_\perp}{\chi_z} = \frac{1 + G_0'}{1 + G_0' + V_{\text{pair}}} = 1 - \frac{V_{\text{pair}}}{1 + G_0' + V_{\text{pair}}}, \quad (11)$$

with the IS pair interaction $V_{\text{pair}} < 0$. For asymmetric systems, there should be a correction due to the neutron excess. A recently developed technique [61] can be used to evaluate this, but it is beyond the scope of the present paper. It is also noted that the dynamic IS pairing affects the p-h type excitation only through the static IV pairing. Within the scope of consideration, roles of the IS pairing can, thus, be investigated only at a minimum. In plotting the ratio $\chi_\perp/\chi_z$, nevertheless, one can expect to see the magnetic properties from different perspectives. Shown in the bottom panel of Fig. 4(a) is the ratio for the Ca isotopes. Since protons do not take part in the spin excitations as mentioned in the beginning, one sees a high asymmetry between χ_z and $\chi_\perp$ even in the case of $N \sim Z$. The enhancement in the ratio $\chi_\perp/\chi_z$ is governed by the shell effect in χ_z and displayed is only a tiny contribution of the dynamic IS pairing to the susceptibility.

Before investigating the Ni isotopes, I am going to discuss briefly how robust the prediction is. Figure 4(b) shows the results obtained by employing the SkP functional. The residual interaction in the spin-isospin channel plays a significant role in the IV-spin excitations. It is noted that the Landau parameter G_0' of the SGII and SkP functionals are 0.93 and 0.06, respectively [62]. The isotopic evolution of the IV-spin susceptibilities is essentially identical to those obtained using the SGII functional, whereas the susceptibilities are predicted to be larger. The enhancement of the susceptibilities is understood by Eq. (9); the SkP functional has a higher effective mass and a weaker residual interaction than SGII.

C. Ni isotopes

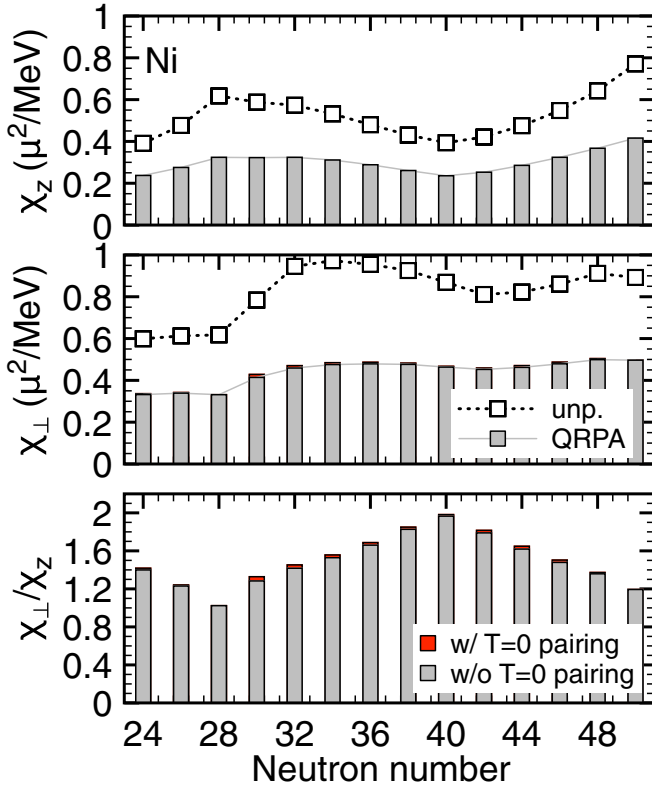An outline of the isotopic dependence of the magnetic properties can be illustrated in the IV-spin susceptibilities χ_z

FIG. 5. As in Fig. 4 but for the Ni isotopes.

FIG. 6. As in Fig. 1 but for the Ni isotopes.

and $\chi_\perp$. Thus, I discuss the isotopic evolution of the collectivity in the spin responses for the Ni isotopes by showing Fig. 5.

Let me discuss first χ_z. In the present case, the $\pi f_{7/2} \to \pi f_{5/2}$ excitation participates in the spin-M1 states in addition to the excitation of neutrons. As in the case for the Ca isotopes, the isotopic evolution of the collectivity is mainly explained by the occupation of neutrons in the $j_>$ orbital. To fortify a conclusion, I show in Fig. 6 the strength distributions of the IV-spin-M1 excitation. A gradual increase in the collectivity up to $N = 28$, enhancement in the transition strength in the giant resonance region, and suppression of the susceptibility due to RPA correlations, is because of the occupation of neutrons in the $f_{7/2}$ orbital. Taking a close look at the strength distribution, one sees that two peaks appear in the giant resonance region in ^{52}Ni, whereas two peaks merge into a single peak in ^{56}Ni. The lower-energy and higher-energy states are mainly generated by the $\pi f_{7/2} \to \pi f_{5/2}$ excitation and the $\nu f_{7/2} \to \nu f_{5/2}$ excitation, respectively. The energy difference for these p-h excitations is about 2 MeV in ^{52}Ni, whereas about 0.2 MeV in ^{56}Ni. Thus, the coherence between these excitations develops from ^{52}Ni to ^{56}Ni. When neutrons occupy the $p_{3/2}$ orbital, a low-lying state shows up. The appearance of the low-lying state has a contribution to the increase in χ_z in $^{50-52}$Ca. In $^{58-60}$Ni, however, the mixing between the $\pi f_{7/2} \to \pi f_{5/2}$ and the $\nu f_{7/2} \to \nu f_{5/2}$ excitations becomes weak, which leads to the cancellation of χ_z. As neutrons occupy the $p_{1/2}$ and $f_{5/2}$ orbitals, the collectivity decreases further. At $N = 40$, the spin excitation is forbidden for neutrons. Beyond $N = 40$, the $\nu g_{9/2} \to \nu g_{7/2}$ excitation starts to

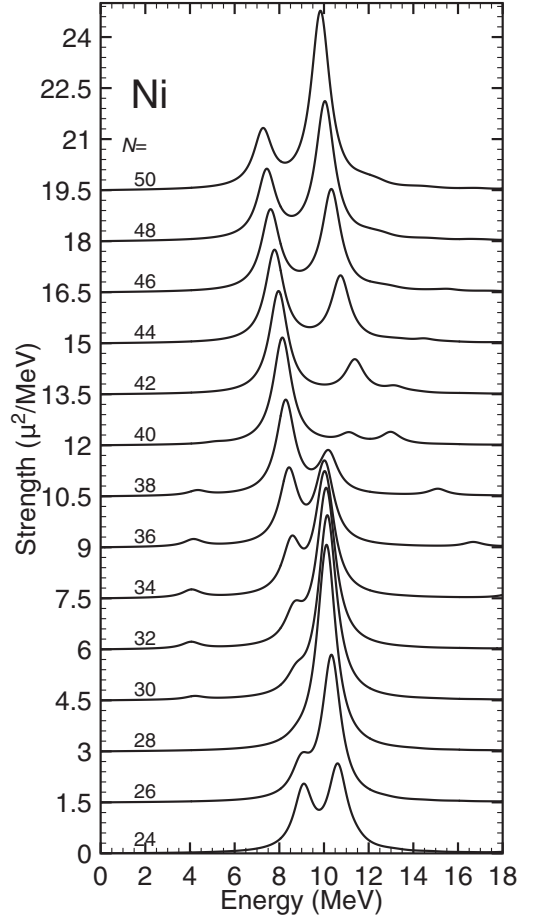appear in the high energy. The lower-energy peak around 8 to 9 MeV and the higher-energy peak around 10 to 11 MeV are predominantly generated by the $\pi f_{7/2} \to \pi f_{5/2}$ excitation and the $\nu g_{9/2} \to \nu g_{7/2}$ excitation, respectively. As in the case for the Ca isotopes, the transition strengths in high energies develop with an increase in the occupation of neutrons in the $g_{9/2}$ orbital.

I then discuss $\chi_\perp$. In $^{52-56}$Ni, the excitation in the t_+ channel has an appreciable contribution to the IV-spin susceptibility as well as that in the t_- channel. Therefore, $\chi_\perp$ value is higher than in the Ca isotopes below $N = 28$. To see what is happening more clearly, I show in Fig. 7(a) the transition strengths in the t_+ channel by the dashed line, where E is replaced by $E_T = E + \lambda^\nu - \lambda^\pi$ in Eq. (6); the transition strengths in the t_- channel are drawn by the solid line. The low-lying state in the t_+ channel is mainly generated by the $\pi f_{7/2} \to \nu f_{7/2}$ excitation. In ^{52}Ni, the neutron occupation probability in the $f_{7/2}$ orbital is 0.48. This configuration is then considered as a hole-hole type excitation and is, thus, affected by the dynamic IS pairing, although not so strongly. The GT state in the t_- channel is constructed by the $\nu f_{7/2} \to \pi f_{5/2}$ excitation, which can be considered as a p-p type excitation at $N = 24$. Since the $\nu f_{7/2} \to \pi f_{7/2}$ excitation is forbidden, the collectivity and the influence by the IS pairing are weaker than in the Ca isotopes.
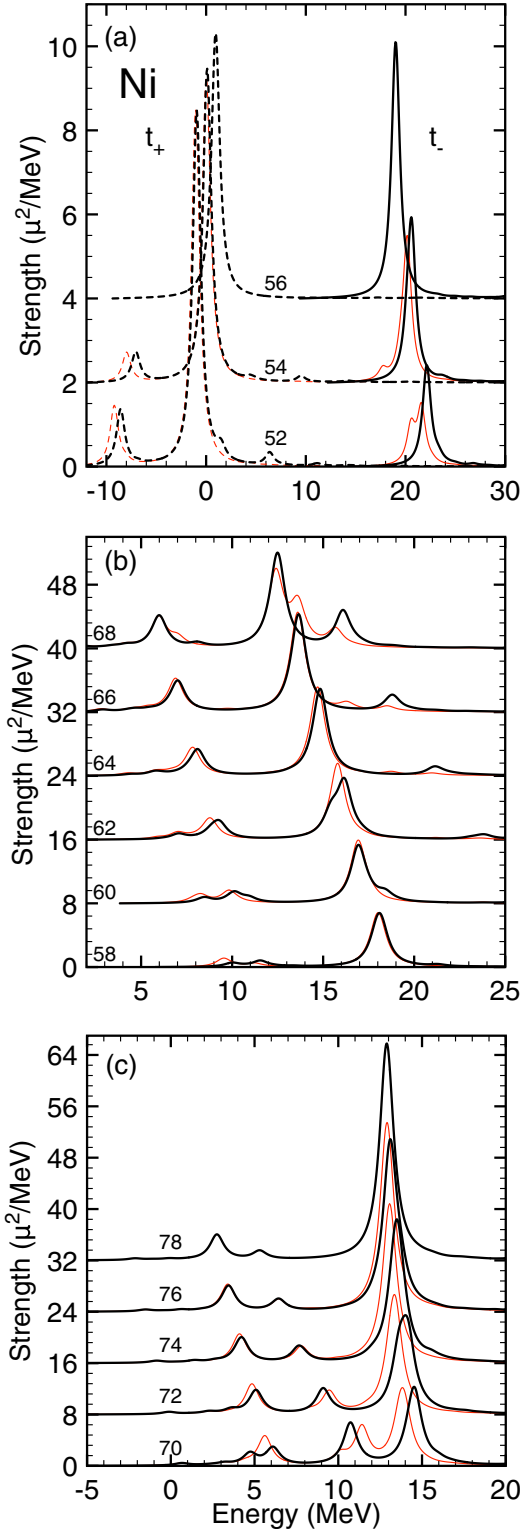
FIG. 7. Similar to Fig. 3 but for (a) $^{52–56}$Ni ($f_{7/2}$ shell), (b) $^{58–68}$Ni ($p – f_{5/2}$ shell) and (c) $^{70–78}$Ni ($g_{9/2}$ shell).

Beyond $N = 28$, one sees in the middle panel of Fig. 5 that the collectivity develops with an increase in the neutron number as in the Ca cases. At $N > 34$, the collectivity does not increase in the Ni isotopes, whereas one has a gradual

increase in the collectivity toward $N = 40$ in the Ca isotopes. This different isotopic dependence results from the fact that the $\nu f_{5/2} \rightarrow \pi f_{7/2}$ excitation does not take part in generating the collectivity due to the Pauli effect in the Ni isotopes. Beyond $N = 40$, the IV-spin susceptibility keeps almost constant similarly in the Ca isotopes because the strength distribution in the low energy is almost unchanged and the $\nu g_{9/2} \rightarrow \pi g_{9/2}$ excitation appears in a high-energy region. Note that the negative-parity states show up instead in the low energy, leading to an interplay between the allowed and the first-forbidden β decays [63]. Since the $\nu g_{9/2} \rightarrow \pi g_{9/2}$ excitation is a p-p type excitation around $N = 40$, the IS pairing affects the giant resonance as shown in Figs. 7(b) and 7(c).

Experimentally, the M1 resonance in ^{58,60,62}Ni has been investigated by several approaches [64–66], and the fragmentation of the strengths was found in the energy region of 8–15 MeV. Similarly, the GT strengths are fragmented in the low energy as well as in the resonance energy region [39,66,67]. Thus, it is not simple to investigate the individual states. Furthermore, the QRPA does not describe the spreading effect originating from the coupling to the 2p2h excitations. Therefore, the sum rule values or the spin susceptibilities are helpful to investigate the magnetic property systematically.

Finally, let me mention the isotopic dependence of the ratio of the IV-spin susceptibilities $\chi_\perp/\chi_z$, showing in the bottom panel of Fig. 5. In ^{56}Ni, its value is unity where protons and neutrons behave symmetrically. Furthermore, the IS pairing is ineffective for the spin susceptibility because of the shell closure. The collectivity becomes stronger above $N = 28$ and stays almost constant beyond $N = 34$ in the charge-exchange channel, whereas that in the neutral channel decreases toward $N = 40$. Then, one sees a gradual increase in the ratio. Beyond $N = 40$, the collectivity is enhanced in the neutral channel, leading to a decrease in the ratio as in the Ca isotopes. The effect of the IS pairing is much weaker than in the case of the Ca isotopes.

IV. SUMMARY

A comparative study on the isotopic dependence of the magnetic properties has been performed by investigating the IV spin-flip excitations in the Ca and Ni isotopes. The responses in the neutral and charge-exchange channels were considered in a unified way. I made use of the nuclear EDF method for calculating the response functions based on the Skyrme-KSB and the QRPA. The like-particle QRPA and the proton-neutron QRPA were employed for the neutral and charge-exchange channels, respectively. The collective shift due to RPA correlations for the response in the neutral channel is mainly explained by the occupation probability of neutrons in the $j_>$ orbital where the IV pairing of neutrons gives a dominant role. In the charge-exchange channel, many p-h or 2qp excitations have a coherent contribution to form a giant resonance in neutron-rich nuclei. The dynamic IS pairing lowers the low-lying and giant resonance states sensitively to the shell structure. I have found that the isotopic evolution

of the collectivity and the shell structure are nicely displayed by the IV-spin susceptibility. A repulsive character of the residual interaction in the spin-isospin channel diminishes the susceptibility, whereas the IS pairing appearing in the charge-exchange channel opposes the suppression.

[1] L. N. Bulaevskii, A. I. Buzdin, M. L. Kulić, and S. V. Panjukov, Coexistence of superconductivity and magnetism theoretical predictions and experimental results, Adv. Phys. **34**, 175 (1985).

[2] J. Schrieffer, *Theory of Superconductivity*, Frontiers in Physics (W. A. Benjamin, San Francisco, 1964).

[3] D. M. Brink and R. A. Broglia, *Nuclear Superfluidity: Pairing in Finite Systems*, Cambridge Monographs on Particle Physics, Nuclear Physics and Cosmology (Cambridge University Press, Cambridge, UK, 2005).

[4] R. Balian and N. R. Werthamer, Superconductivity with pairs in a relative p wave, Phys. Rev. **131**, 1553 (1963).

[5] A. J. Leggett, Spin Susceptibility of A Superfluid Fermi Liquid, Phys. Rev. Lett. **14**, 536 (1965).

[6] D. Vollhardt and P. Wolfle, *The Superfluid Phases of Helium 3* (Taylor and Francis, New York, 1990).

[7] R. Joynt and L. Taillefer, The superconducting phases of UPt$_3$, Rev. Mod. Phys. **74**, 235 (2002).

[8] A. P. Mackenzie and Y. Maeno, The superconductivity of Sr$_2$RuO$_4$ and the physics of spin-triplet pairing, Rev. Mod. Phys. **75**, 657 (2003).

[9] S. Frauendorf and A. O. Macchiavelli, Overview of neutron–proton pairing, Prog. Part. Nucl. Phys. **78**, 24 (2014).

[10] P. Haensel, A. Potekhin, and D. Yakovlev, *Neutron Stars 1: Equation of State and Structure*, Astrophysics and Space Science Library (Springer, New York, 2007).

[11] M. Harakeh and A. Woude, *Giant Resonances: Fundamental High-frequency Modes of Nuclear Excitation* (Oxford University Press, Oxford, 2001).

[12] K. Yoshida, Proton-neutron pairing vibrations in $N = Z$ nuclei: Precursory soft mode of isoscalar pairing condensation, Phys. Rev. C **90**, 031303(R) (2014).

[13] E. Litvinova, C. Robin, and I. A. Egorova, Soft modes in the proton–neutron pairing channel as precursors of deuteron condensate in $N = Z$ nuclei, Phys. Lett. B **776**, 72 (2018).

[14] Y. Chazono, K. Yoshida, K. Yoshida, and K. Ogata, Proton induced deuteron knockout reaction as a probe of an isoscalar proton-neutron pair in nuclei, Phys. Rev. C **103**, 024609 (2021).

[15] M. Ericson, Nuclear spin/isospin response functions, Prog. Part. Nucl. Phys. **11**, 277 (1984).

[16] F. Osterfeld, Nuclear spin and isospin excitations, Rev. Mod. Phys. **64**, 491 (1992).

[17] K. Heyde, P. von Neumann-Cosel, and A. Richter, Magnetic dipole excitations in nuclei: elementary modes of nucleonic motion, Rev. Mod. Phys. **82**, 2365 (2010).

[18] S. X. Nakamura, H. Kamano, Y. Hayato, M. Hirai, W. Horiuchi, S. Kumano, T. Murata, K. Saito, M. Sakuda, T. Sato, and Y. Suzuki, Towards a unified model of neutrino-nucleus reactions for neutrino oscillation experiments, Rep. Prog. Phys. **80**, 056301 (2017).

[19] F. Käppeler, R. Gallino, S. Bisterzo, and W. Aoki, The s process: Nuclear physics, stellar models, and observations, Rev. Mod. Phys. **83**, 157 (2011).

[20] M. Arnould, S. Goriely, and K. Takahashi, The r-process of stellar nucleosynthesis: Astrophysics and nuclear physics achievements and mysteries, Phys. Rep. **450**, 97 (2007).

[21] T. Kajino, W. Aoki, A. B. Balantekin, R. Diehl, M. A. Famiano, and G. J. Mathews, Current status of r -process nucleosynthesis, Prog. Part. Nucl. Phys. **107**, 109 (2019).

[22] N. Auerbach and A. Klein, Structure of isovector spin excitations in nuclei, Phys. Rev. C **30**, 1032 (1984).

[23] J. Engel, M. Bender, J. Dobaczewski, W. Nazarewicz, and R. Surman, Beta decay of r-process waiting-point nuclei in a self-consistent approach, Phys. Rev. C **60**, 014302 (1999).

[24] K. Yoshida, Spin–isospin response of deformed neutron-rich nuclei in a self-consistent Skyrme energy-density-functional approach, Prog. Theor. Exp. Phys. **2013**, 113D02 (2013); **2021**, 019201(E) (2021).

[25] Y. Tanimura, H. Sagawa, and K. Hagino, Three-body model calculations for $N = Z$ odd–odd nuclei with $T = 0$ and $T = 1$ pairing correlations, Prog. Theor. Exp. Phys. **2014**, 53D02 (2014).

[26] C. L. Bai, H. Sagawa, G. Colò, Y. Fujita, H. Q. Zhang, X. Z. Zhang, and F. R. Xu, Low-energy collective Gamow-Teller states and isoscalar pairing interaction, Phys. Rev. C **90**, 054335 (2014).

[27] H. Fujita, Y. Fujita, Y. Utsuno, K. Yoshida, T. Adachi, A. Algora, M. Csatlós, J. M. Deaven, E. Estevez-Aguado, C. J. Guess, J. Gulyás, K. Hatanaka, K. Hirota, R. Hutton, D. Ishikawa, A. Krasznahorkay, H. Matsubara, F. Molina, H. Okamura, H. J. Ong *et al.*, Experimental study of Gamow-Teller transitions via the high-energy-resolution ^{18}O(^{3}He, t) ^{18}F reaction: Identification of the low-energy "super" -Gamow-Teller state, Phys. Rev. C **100**, 034618 (2019).

[28] Y. Fujita, H. Fujita, T. Adachi, C. L. Bai, A. Algora, G. P. A. Berg, P. von Brentano, G. Colò, M. Csatlós, J. M. Deaven, E. Estevez-Aguado, C. Fransen, D. De Frenne, K. Fujita, E. Ganioğlu, C. J. Guess, J. Gulyás, K. Hatanaka, K. Hirota, M. Honma *et al.*, Observation of Low- and High-Energy Gamow-Teller Phonon Excitations in Nuclei, Phys. Rev. Lett. **112**, 112502 (2014).

[29] Y. Fujita, H. Fujita, T. Adachi, G. Susoy, A. Algora, C. L. Bai, G. Colò, M. Csatlós, J. M. Deaven, E. Estevez-Aguado, C. J. Guess, J. Gulyás, K. Hatanaka, K. Hirota, M. Honma, D. Ishikawa, A. Krasznahorkay, H. Matsubara, R. Meharchand, F. Molina *et al.*, High-resolution study of Gamow-Teller excitations in the ^{42}Ca(^{3}He, t) ^{42}Sc reaction and the observation of a "low-energy super-Gamow-Teller state", Phys. Rev. C **91**, 064316 (2015).

[30] M. Bender, P.-H. Heenen, and P.-G. Reinhard, Self-consistent mean-field models for nuclear structure, Rev. Mod. Phys. **75**, 121 (2003).

[31] T. Nakatsukasa, K. Matsuyanagi, M. Matsuo, and K. Yabana, Time-dependent density-functional description of nuclear dynamics, Rev. Mod. Phys. **88**, 045004 (2016).

[32] K. Yoshida and N. V. Giai, Deformed quasiparticle-random-phase approximation for neutron-rich nuclei using the Skyrme energy density functional, Phys. Rev. C **78**, 064316 (2008).

[33] K. Yoshida and T. Nakatsukasa, Shape evolution of giant resonances in Nd and Sm isotopes, Phys. Rev. C **88**, 034309 (2013).

[34] J. Dobaczewski, H. Flocard, and J. Treiner, Hartree-Fock-Bogolyubov description of nuclei near the neutron-drip line, Nucl. Phys. A **422**, 103 (1984).

[35] H. Kasuya and K. Yoshida, Hartree–Fock–Bogoliubov theory for odd-mass nuclei with a time-odd constraint and application to deformed halo nuclei, Prog. Theor. Exp. Phys. **2021**, 013D01 (2021).

[36] N. van Giai and H. Sagawa, Spin-isospin and pairing properties of modified Skyrme interactions, Phys. Lett. B **106**, 379 (1981).

[37] M. Yamagami, Y. R. Shimizu, and T. Nakatsukasa, Optimal pair density functional for description of nuclei with large neutron excess, Phys. Rev. C **80**, 064301 (2009).

[38] A. Richter, A. Weiss, O. Haüsser, and B. A. Brown, New Evidence for Meson-Exchange-Current Enhancement of Isovector M1 Strength, Phys. Rev. Lett. **65**, 2519 (1990).

[39] Y. Fujita, B. Rubio, and W. Gelletly, Spinisospin excitations probed by strong, weak and electro-magnetic interactions, Prog. Part. Nucl. Phys. **66**, 549 (2011).

[40] D. Pringle, E. Garman, S. Chew, K. Snover, W. Catford, S. Hesmondhalgh, and K. Allen, Decay of the lowest $T = 2$ state in ^{40}Ca, Phys. Lett. B **115**, 291 (1982).

[41] S. P. Kamerdzhiev and V. N. Tkachev, A microscopic model taking into account 2p2h configurations in magic nuclei. Calculations of M1 excitations, Z. Phys. A **334**, 19 (1989).

[42] A. Bohr and B. Mottelson, *Nuclear Structure: Volume II, Nuclear Deformations* (Benjamin, New York, 1975).

[43] W. Steffen, H.-D. Grf, W. Gross, D. Meuer, A. Richter, E. Spamer, O. Titze, and W. Knpfer, Backward-angle high-resolution inelastic electron scattering on ^{40,42,44,48}Ca and observation of a very strong magnetic dipole ground-state transition in ^{48}Ca, Phys. Lett. B **95**, 23 (1980).

[44] I. Hamamoto and H. Sagawa, Response of light drip line nuclei to spin dependent operators, Phys. Rev. C **60**, 064314 (1999).

[45] S. Kamerdzhev, J. Speth, G. Tertychny, and J. Wambach, M1 resonances in unstable magic nuclei, Z. Phys. A **346**, 253 (1993).

[46] T. Oishi, G. Kružić, and N. Paar, Role of residual interaction in the relativistic description of M1 excitation, J. Phys. G: Nucl. Part. Phys. **47**, 115106 (2020).

[47] M. Matsuo, Continuum linear response in coordinate space Hartree-Fock-Bogoliubov formalism for collective excitations in dripline nuclei, Nucl. Phys. A **696**, 371 (2001).

[48] M. Matsuo, K. Mizuyama, and Y. Serizawa, Di-neutron correlation and soft dipole excitation in medium mass neutron-rich nuclei near drip-line, Phys. Rev. C **71**, 064326 (2005).

[49] K. Yoshida, M. Yamagami, and K. Matsuyanagi, Dynamic pairing effects on low-frequency modes of excitation in deformed Mg isotopes close to the neutron drip line, Phys. Scr. **T125**, 45 (2006).

[50] K. Yoshida, M. Yamagami, and K. Matsuyanagi, Pairing and continuum effects on low-frequency quadrupole vibrations in deformed Mg isotopes close to the neutron drip line, Nucl. Phys. A **779**, 99 (2006).

[51] K. Yoshida and M. Yamagami, Low-frequency $K^\pi = 0^+$ modes in deformed neutron-rich nuclei: Pairing- and β-vibrational modes of neutron, Phys. Rev. C **77**, 044312 (2008).

[52] K. Yoshida, Pairing and nonaxial-shape correlations in $N = 150$ isotones, arXiv:2105.03128.

[53] E. Lipparini and S. Stringari, Sum rules and giant resonances in nuclei, Phys. Rep. **175**, 103 (1989).

[54] W. Alberico, A. Molinari, R. Cenni, and M. B. Johnson, On the collective modes of infinite nuclear matter, Ann. Phys. (NY) **138**, 178 (1982).

[55] S. Belyaev, Time-dependent self-consistent field and collective nuclear Hamiltonian, Nucl. Phys. **64**, 17 (1965).

[56] H. Sagawa, C. L. Bai, and G. Colò, Isovector spin-singlet ($T = 1$, $S = 0$) and isoscalar spin-triplet ($T = 0$, $S = 1$) pairing interactions and spin-isospin response, Phys. Scr. **91**, 083011 (2016).

[57] Y. Fujita, T. Adachi, H. Fujita, A. Algora, B. Blank, M. Csatlós, J. M. Deaven, E. Estevez-Aguado, E. Ganioğlu, C. J. Guess, J. Gulyás, K. Hatanaka, K. Hirota, M. Honma, D. Ishikawa, A. Krasznahorkay, H. Matsubara, R. Meharchand, F. Molina, H. Okamura *et al.*, High-resolution study of $T_z = +2 \rightarrow +1$ Gamow-Teller transitions in the ^{44}Ca(^{3}He, t)^{44}Sc reaction, Phys. Rev. C **88**, 014308 (2013).

[58] E.-W. Grewe, D. Frekers, S. Rakers, T. Adachi, C. Bäumer, N. T. Botha, H. Dohmann, H. Fujita, Y. Fujita, K. Hatanaka, K. Nakanishi, A. Negret, R. Neveling, L. Popescu, Y. Sakemi, Y. Shimbara, Y. Shimizu, F. D. Smit, Y. Tameshige, A. Tamii *et al.*, (^{3}He, t) reaction on the double β decay nucleus ^{48}Ca and the importance of nuclear matrix elements, Phys. Rev. C **76**, 054307 (2007).

[59] H. Sagawa, I. Hamamoto, and M. Ishihara, Gamow-Teller states in light nuclei near the neutron drip line, Phys. Lett. B **303**, 215 (1993).

[60] K. Yoshida, Charge-exchange dipole excitations in neutron-rich nuclei: $-1\hbar\omega_0$, anti-analog pygmy and anti-analog giant resonances, Phys. Rev. C **96**, 051302(R) (2017).

[61] D. Davesne, A. Pastore, and J. Navarro, Linear response theory in asymmetric nuclear matter for Skyrme functionals including spin-orbit and tensor terms II: Charge Exchange, Phys. Rev. C **100**, 064301 (2019).

[62] M. Bender, J. Dobaczewski, J. Engel, and W. Nazarewicz, Gamow-Teller strength and the spin-isospin coupling constants of the Skyrme energy functional, Phys. Rev. C **65**, 054322 (2002).

[63] K. Yoshida, Suddenly shortened half-lives beyond ^{78}Ni: $N = 50$ magic number and high-energy non-unique first-forbidden transitions, Phys. Rev. C **100**, 024316 (2019).

[64] R. A. Lindgren, W. L. Bendel, E. C. Jones, L. W. Fagg, X. K. Maruyama, J. W. Lightbody, and S. P. Fivozinsky, Electroexcitation of the $T_0 + 1$ giant $M1$ resonance in ^{58,60}Ni, Phys. Rev. C **14**, 1789 (1976).

[65] W. Mettner, A. Richter, W. Stock, B. Metsch, and A. Van Hees, Electroexcitation of ^{58}Ni: A sutdy of the fragmentation of the magnetic dipole strength, Nucl. Phys. A **473**, 160 (1987).

[66] H. Fujita, Y. Fujita, T. Adachi, A. D. Bacher, G. P. A. Berg, T. Black, E. Caurier, C. C. Foster, H. Fujimura, K. Hara, K. Harada, K. Hatanaka, J. Jänecke, J. Kamiya, Y. Kanzaki, K. Katori, T. Kawabata, K. Langanke, G. Martínez-Pinedo, T. Noro

et al., Isospin structure of $J^\pi = 1^+$ states in ^{58}Ni and ^{58}Cu studied by ^{58}Ni(p, p') and ^{58}Ni$(^3$He$, t)^{58}$Cu measurements, Phys. Rev. C **75**, 034310 (2007).

[67] L. Popescu, T. Adachi, G. P. A. Berg, P. von Brentano, D. Frekers, D. De Frenne, K. Fujita, Y. Fujita, E.-W. Grewe, M. N.

Harakeh, K. Hatanaka, E. Jacobs, K. Nakanishi, A. Negret, Y. Sakemi, Y. Shimbara, Y. Shimizu, Y. Tameshige, A. Tamii, M. Uchida *et al.*, Gamow-Teller transitions studied in the high-resolution ^{64}Ni$(^3$He$, t)^{64}$Cu reaction, Phys. Rev. C **79**, 064312 (2009).